Bol. Soc. Paran. Mat.
©SPM – E-ISSN-2175-1188
SPM: www.spm.uem.br/bspm

(3s.) **v. 2026 (44) 11** : 1–20.
ISSN-0037-8712
doi:10.5269/bspm.78301

Heat Transfer and Entrance Flow Characteristics of Viscoplastic Fluid in a Circular Cylinder Using the Bingham-Papanastasiou Model

Deepa Madivalar*, Vishwanath Kadaba Puttanna, A. Kandasamy

ABSTRACT: This study investigates the laminar flow of an incompressible viscoplastic fluid in the entrance region of a circular cylinder, with emphasis on heat transfer characteristics by considering two different thermal boundary conditions: constant wall temperature and constant wall heat flux. The fluid behavior is modeled using the regularized Bingham-Papanastasiou approach, and the analysis is conducted under the assumptions of Prandtl's boundary layer theory using the finite difference method. The study highlights the simultaneous development of the velocity and thermal boundary layers. It presents a detailed analysis of the heat transfer behavior of Bingham fluid flow in the cylindrical geometry. The impact of yield stress on the flow and thermal parameters is thoroughly examined. The presence of yield stress significantly affects flow characteristics such as velocity, pressure, and temperature distributions. It also influences heat transfer performance, particularly the Nusselt number. The effects of key dimensionless parameters, such as the Bingham and the Prandtl number, are also discussed. The obtained results are consistent with previously reported findings in certain limiting cases, validating the current approach.

Keywords: Viscoplastic fluid, circular cylinder, entrance region, Bingham-Papanastasiou Model, FDM, Bingham number, Prandtl number, Nusselt number.

Contents

1. Introduction

The simultaneous development of the velocity boundary layer and thermal boundary layer in the entrance region of laminar flow through a circular cylinder has been extensively studied for various types of fluids [14]. This problem is highly relevant to numerous engineering applications, particularly in the design of heat exchangers [31].

In the case of Newtonian fluids, several studies have analyzed this problem through various numerical and analytical approaches [5,11,4]. Further, in many cases, some of these fluids exhibit solid-like behavior below a critical stress called yield stress, but begin to flow once this threshold is exceeded. These fluids are commonly known as viscoplastic fluids. This characteristic influences the designing process of the materials.

* Corresponding author.
2020 *Mathematics Subject Classification:* 35B40, 35L70.
Submitted August 07, 2025. Published March 13, 2026

Previous studies have examined laminar flow in the entrance regions of various geometries—such as cylinders, annuli, and channels—for viscoplastic fluids [22,23,19,7,27,34,24,15,20,13,1,8,32,10,28]. The common interest amongst these investigations was the entry length. The entry length is typically defined as the distance required for the velocity to attain 99% of its fully developed value, as given in [22]. However, several studies have proposed modifications to this definition. For instance, Ookawara et al. [23] revised the definition for the developing length at low Reynolds numbers for cylinder flow, characterizing it as the axial distance where the velocity reaches 99% of its fully developed value at a radial position corresponding to 95% of the plug radius. Due to computational limitations, their study did not explore cases with smaller relative plug radii.

Later, Poole and Chhabra [27] used the same definition of entry length and investigated the entry length of Bingham fluids under creeping flow conditions using both the biviscosity model and the regularized Papanastasiou model. They employed the SIMPLER algorithm to solve the governing equations. Their findings showed that, at high Reynolds numbers, the entry length behavior of Bingham fluids closely follows that of Newtonian fluids. However, this alignment fails to occur when the Reynolds number is low.

Pai and Kandasamy [24] analytically studied the entrance region flow behavior in an annular geometry by applying mass conservation and momentum equations along with the ideal Bingham fluid model. Their study focused on the plug core region and the entry length of viscoplastic fluid flow. Further investigations into the entrance region of viscoplastic fluid flow for high-yield stress fluids with the assumption of flow everywhere in an annular geometry were carried out by Kandasamy and Nadiminti [15]. They utilized Prandtl's boundary layer assumptions with the ideal Bingham model and a finite difference scheme to examine the tangential, radial, and axial flow characteristics of viscoplastic fluids in a concentric annulus.

Recently, Baioumy et al. [1] employed the boundary layer approach in conjunction with the momentum integral method and used the ideal Bingham model to analyze Bingham fluid flow. Their results show that the boundary layer thickness grows until the plug flow region becomes fully developed. Additionally, they observed changes in pressure drop and centerline velocity at lower yield stress values. Subsequently, Syrakos et al. [32] revisited the entry length of viscoplastic fluids using the regularized Papanastasiou model within a finite element framework. They proposed alternative definitions for both the developing length and the Reynolds number, highlighting the dependence of the entry length on yield stress, the regularization parameter, and the Reynolds number. Additionally, Philippou [26] investigated viscoplastic flow in pipes and channels with wall slip. Building on this, Gryparis et al. [10] addressed a similar problem by analyzing flow in annular tubes under wall slip conditions.

The flow behavior of viscoplastic and Newtonian fluids in the entrance region of different geometries plays a crucial role in determining heat transfer performance [3,21,17,9,2]. Therefore, it is essential to examine both the thermal and hydrodynamic boundary layers simultaneously, focusing on the flow parameters-velocity and temperature at the inlet of the domain for a comprehensive understanding. Most research in this area has focused on three-dimensional computational simulations for heat transfer problems. This was initially investigated by Vradis et al. [33], who studied Bingham fluid flow in a circular pipe under constant wall temperature. They conducted a three-dimensional computational simulation using the finite difference method and the bi-viscosity model. Their results revealed that the developed velocity decreases with increasing yield number, and the Nusselt number is higher when viscous dissipation effects are considered compared to cases where these effects are neglected. Later, Min et al. [18] studied the convective heat transfer of Bingham plastic in a circular pipe by incorporating a viscous dissipation term using a fractional method. They presented the heat transfer characteristics of Bingham fluids throughout the pipe, applying the Bingham Papanastasiou model. Labsi et al. [17] analyzed temperature-dependent viscosity for pipe flow with the Papanastasiou model and finite element method. Their results show that the pressure drop is significant for constant plastic viscosity cases, and the Nusselt number increases as the temperature difference rises for both heating and cooling scenarios.

Soares et al. [30] investigated the heat transfer behavior of Herschel-Bulkley fluids in the entrance region of a pipe, neglecting viscous dissipation under two different thermal boundary conditions: uniform wall heat flux and uniform wall temperature. Using the bi-viscosity model and implementing the finite volume method, they demonstrated that the Nusselt number in the entrance region is consistently higher for the case with uniform wall heat flux than that with uniform wall temperature. Later, E. J. Soares

et al. [29] analyzed the same approach for the flow in the concentric annuli, and the results show that a higher velocity gradient will give a higher Nusselt number.

From the above works, it is observed that the flow of viscoplastic fluids in various geometries has been analyzed using three-dimensional simulations. Various authors have used different constitutive equations to represent Bingham fluid flow, like the ideal Bingham model, the bi-viscosity model, and the regularized Papanastasiou model. Among these models, the Papanastasiou model provides a better understanding of viscoplastic fluid behavior, as it provides better insights into the flow of yield stress fluids through computational analysis. Even though some of the works used the regularized Papanastasiou model, not much work has been reported in the entrance region analysis using boundary layer assumptions.

We intend to investigate the effects of heat transfer in the entrance region of a circular cylinder using the Bingham-Papanastasiou model, based on the assumption of Prandtl's boundary layer theory, and consider two thermal boundary conditions: constant wall temperature and constant wall heat flux. This type of analysis is particularly important in various industrial applications involving the flow of viscoplastic fluids, such as in the food, paint, pharmaceutical, cosmetic, and petroleum industries [16].

First, we formulate the boundary layer equations based on appropriate assumptions. Next, we present the finite difference scheme along with its corresponding finite difference forms of the equations. We then describe the solution technique, followed by the presentation of results, which include velocity, pressure, temperature, bulk temperature, and the Nusselt number. These results are compared with findings from previous studies for some particular cases.

2. Mathematical Formulation

Consider the laminar flow of a viscoplastic Bingham fluid in the entrance region of a horizontal circular cylinder. The fluid enters the horizontal cylinder, which has a radius r_1, with a uniform initial velocity u_0 and pressure p_0, while a no-slip condition is imposed at the cylinder walls. The focus of this study is to investigate heat transfer based on two thermal boundary conditions, viz., temperature is constant at the wall and heat flux is constant at the wall, as depicted in Figure 1.

Assuming the flow to be incompressible, laminar, steady with constant fluid physical properties, we can neglect the diffusion of heat in the axial direction and any viscous dissipation. Based on these assumptions, the Prandtl boundary layer equations for this fluid problem in cylindrical coordinates (r, x) are given as follows [6]:

Figure 1: Entrance Region Flow of Cylinder

$$\frac{\partial v_x}{\partial x} + \frac{1}{r}\frac{\partial (r v_r)}{\partial r} = 0 \tag{2.1}$$

$$\rho\left[v_x\frac{\partial v_x}{\partial x} + v_r\frac{\partial v_x}{\partial r}\right] = -\frac{\partial p}{\partial x} + \frac{1}{r}\frac{\partial (r\tau_{rx})}{\partial r} \tag{2.2}$$

$$\rho c_p\left[v_x\frac{\partial T}{\partial x} + v_r\frac{\partial T}{\partial r}\right] = k\left[\frac{1}{r}\frac{\partial}{\partial r}\left(r\frac{\partial T}{\partial r}\right)\right] \tag{2.3}$$

In this context, v_x and v_r denote the velocity components in the axial(x) and radial(r) directions, respectively, while p represents the pressure, T is the temperature, and ρ is the fluid density. The thermal parameters of the fluid, namely, the specific heat capacity and thermal conductivity are denoted by c_p and k, respectively. The term τ_{rx} refers to the shear stress acting in the axial (x) direction on a surface perpendicular to the radial (r) direction, and its value depends on the fluid's rheological behavior.

The constitutive equation for the ideal Bingham model to explain the viscoplastic behavior is

$$\begin{cases} \tau_{rx} = \tau_0 + \mu_p \dfrac{\partial v_x}{\partial r} & \text{if } \tau_{rx} > \tau_0 \\ \dfrac{\partial v_x}{\partial r} = 0 & \text{if } \tau_{rx} \leq \tau_0 \end{cases} \tag{2.4}$$

Here, τ_0 denotes the fluid's yield stress. In this model (2.4), the tracking of the yield surface is completely eliminated for viscoplastic fluid flow. To overcome this problem, Papanastasiou proposed a model [25] that provides a continuous viscoplastic equation, which is valid in both yielded and unyielded regions.

$$\tau_{rx} = \left[\frac{\tau_0[1 - exp(-m|\frac{\partial v_x}{\partial r}|)]}{|\frac{\partial v_x}{\partial r}|} + \mu_p \right] \frac{\partial v_x}{\partial r} \tag{2.5}$$

The variable m represents the exponent term that regulates stress growth. In the limit as $m \to 0$, the fluid behaves like a Newtonian fluid, whereas as $m \to \infty$, behavior is that of the ideal Bingham model (2.4). Substituting this regularized constitutive Equation (2.5) in Equation (2.2) we get,

$$\rho \left[v_x \frac{\partial v_x}{\partial x} + v_r \frac{\partial v_x}{\partial r} \right] = -\frac{\partial p}{\partial x} + \frac{1}{r} \frac{\partial}{\partial r} \left[r \left(\frac{\tau_0[1 - exp(-m|\frac{\partial v_x}{\partial r}|)]}{|\frac{\partial v_x}{\partial r}|} + \mu_p \right) \frac{\partial v_x}{\partial r} \right] \tag{2.6}$$

Based on the flow configuration in Figure 1, the boundary conditions for the velocity and pressure are given below in Equation (2.7),

$$\begin{aligned} &\text{At } x = 0 \text{ and } 0 < r < r_1 : && v_x = u_0, \quad v_r = 0 \\ &\text{At } x = 0 : && p = p_0 \\ &\text{For } x \geq 0 \text{ and } r = 0 : && \frac{\partial v_x}{\partial r} = 0, \quad v_r = 0 \\ &\text{For } x \geq 0 \text{ and } r = r_1 : && v_x = 0, \quad v_r = 0 \end{aligned} \tag{2.7}$$

For a constant wall temperature, the thermal boundary conditions in [30] for the Equation (2.3) are

$$T(r, 0) = T_o, \quad \frac{\partial T}{\partial r}(0, x) = 0, \quad T(r_1, x) = T_w; \tag{2.8}$$

while, for constant wall heat flux, the thermal boundary conditions should be written as

$$T(r, 0) = T_o, \quad \frac{\partial T}{\partial r}(0, x) = 0, \quad k\frac{\partial T}{\partial r}(r_1, x) = q; \tag{2.9}$$

Using these velocity boundary conditions in Equation (2.7), the equation of continuity (2.1) in the integral form can be written as

$$\int_0^{r_1} 2\pi r v_x \, dr = \pi r_1^2 u_0. \tag{2.10}$$

The equations (2.1), (2.6), (2.3), and (2.10) along with the boundary conditions from equations

(2.7), (2.8),and (2.9) are non-dimensionalized using the following dimensionless parameters:

$$\begin{gathered} U=\frac{v_x}{u_0}, \quad R=\frac{r}{r_1}, \quad P=\frac{p-p_0}{\rho u_0^2}, \quad V=\frac{\rho v_r r_1}{\mu_p}, \quad X=\frac{2x}{r_1 \mathrm{Re}}, \\ M=\frac{m u_0}{r_1}, \quad B=\frac{\tau_0 r_1}{u_0 \mu_p}, \quad \mathrm{Re}=\frac{2\rho r_1 u_0}{\mu_p}, \quad \mathrm{Pr}=\frac{\mu_p c_p}{k}, \\ \theta=\begin{cases} \dfrac{T-T_0}{T_w-T_0}, & \text{for constant wall temperature,} \\ \dfrac{k}{q r_1}(T-T_0), & \text{for constant wall heat flux.} \end{cases} \end{gathered} \tag{2.11}$$

Here, B is the Bingham number, M is the regularization parameter, Re is the Reynolds number, and Pr is the Prandtl number.

Based on the non-dimensional parameters in (2.11), the dimensionless forms of the equations (2.1), (2.6), (2.3), and (2.10) can be written as follows:

$$\frac{\partial U}{\partial X}+\frac{1}{R}\frac{\partial (RV)}{\partial R} = 0 \tag{2.12}$$

$$U\frac{\partial U}{\partial X}+V\frac{\partial U}{\partial R} = -\frac{dP}{dX}+\frac{1}{R}\frac{\partial}{\partial R}\left\{R\left[1+\frac{\mathbf{B}\left(1-exp(-\mathbf{M}|\frac{\partial U}{\partial R}|)\right)}{|\frac{\partial U}{\partial R}|}\right]\frac{\partial U}{\partial R}\right\} \tag{2.13}$$

$$U\frac{\partial \theta}{\partial X}+V\frac{\partial \theta}{\partial R} = \frac{1}{Pr}\left\{\frac{\partial^2 \theta}{\partial R^2}+\frac{1}{R}\frac{\partial \theta}{\partial R}\right\} \tag{2.14}$$

$$\int_0^1 UR\,dR = \frac{1}{2} \tag{2.15}$$

and the corresponding dimensionless boundary conditions are as follows,

$$\begin{aligned} &\text{At } X=0 \text{ and } 0<R<1: && U=1, \quad V=0 \\ &\text{At } X=0: && P=0 \\ &\text{For } X\geq 0 \text{ and } R=0: && \frac{\partial U}{\partial R}=0, \quad V=0 \\ &\text{For } X\geq 0 \text{ and } R=1: && U=0, \quad V=0 \end{aligned} \tag{2.16}$$

The non-dimensional thermal boundary conditions [30] for constant wall temperature are given by,

$$\theta(R,0)=0, \quad \frac{\partial \theta}{\partial R}(0,X)=0, \quad \text{and} \quad \theta(1,X)=1. \tag{2.17}$$

and for constant wall heat flux,

$$\theta(R,0)=0, \quad \frac{\partial \theta}{\partial R}(0,X)=0, \quad \text{and} \quad \frac{\partial \theta}{\partial R}(1,X)=1. \tag{2.18}$$

The set of equations (2.12) - (2.15) along with the boundary conditions from equations (2.16),(2.17), and (2.18) can be solved to determine flow parameters such as velocity, pressure and temperature, using the method of finite differences described in the following section.

3. Methodology

The finite Difference Method (FDM), described by Hornbeck [12], includes the necessary boundary conditions. Figure 2 illustrates the grid generation process in the axial direction, which uses a step length of 10^{-6} from 0 to 0.1, and a step length of 2.5×10^{-5} from 0.1 onward. A step length of 0.002 is utilized in the radial direction. At a given point (i,j), the values of the flow parameters are assumed to be known,

while those at $(i, j+1)$ remain unknown. This method utilizes a central difference scheme in the radial direction and a backward difference scheme in the axial direction. Finite difference approximations are applied to dimensionless Equations (2.12), (2.13), (2.14), and (2.15) at location $(i, j+1)$. The subsequent sections discuss the application of FDM in solving the hydrodynamic and thermal aspects of the problem.

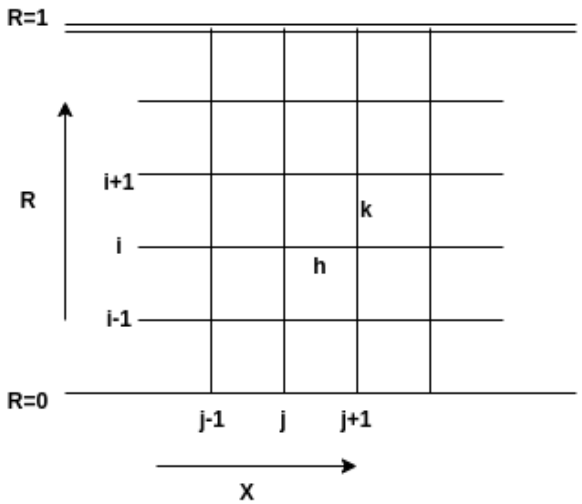

Figure 2: Finite Difference Scheme

3.1. Computing Velocities and Pressure drop in Flow Domain

The hydrodynamic aspect of the problem is addressed using the non-dimensional continuity equation (2.12), the x-momentum equation (2.13), and the integral form (2.15) using the following finite difference scheme computationally with extension of work in [12].

The finite difference form of the continuity equation is given.

$$\frac{U_{i+1,j+1} - U_{i+1,j} + U_{i,j+1} - U_{i,j}}{2\Delta X} + \frac{1}{R_i}\frac{V_{i+1,j+1}R_{i+1} - V_{i,j+1}R_i}{\Delta R} = 0 \tag{3.1}$$

which on simplification can be written as,

$$V_{i+1,j+1} = V_{i,j+1}\left(\frac{R_i}{R_{i+1}}\right) - \frac{\Delta R}{2\Delta X}\left(\frac{R_i}{R_{i+1}}\right)[U_{i+1,j+1} - U_{i+1,j} + U_{i,j+1} - U_{i,j}] \tag{3.2}$$

The finite difference form of the x-momentum equation

$$P_{j+1} + U_{i-1,j+1}\left[\frac{\Delta X B_1}{2(\Delta R)R_i} - \frac{(\Delta X)V_{i,j}}{2(\Delta R)} - \frac{(\Delta X)B_2}{(\Delta R)^2}\right] + U_{i,j+1}\left[U_{i,j} + \frac{2(\Delta X)B_2}{(\Delta R)^2}\right]$$

$$+ U_{i+1,j+1}\left[-\frac{\Delta X B_1}{2(\Delta R)R_i} + \frac{(\Delta X)V_{i,j}}{2(\Delta R)} - \frac{(\Delta X)B_2}{(\Delta R)^2}\right] = (U_{i,j})^2 + P_j \tag{3.3}$$

here $B_1 = 1 + \dfrac{B[1 - exp(-M|\frac{\partial U}{\partial R}|)]}{|\frac{\partial U}{\partial R}|}$

$B_2 = 1 + BMexp\left(-M\left|\dfrac{\partial U}{\partial R}\right|\right)$

$\left|\dfrac{\partial U}{\partial R}\right| = \left|\dfrac{U_{i+1,\ j} - U_{i-1,\ j}}{2\Delta R}\right|$

The integral equation reduces to,

$$\sum_{i=0}^{n} R_i U_{i,j+1} = \sum_{i=0}^{n} R_i U_{i,j} \tag{3.4}$$

In the hydrodynamic part, the variables (U, V, P) are the unknowns that need to be determined. To find these unknowns, the linearized set of Equations (3.3) and (3.4) are solved using the Gauss elimination method to obtain U and P in each cross-section. The value of V is explicitly determined using the U values from previous calculations and solving the continuity Equation (3.2). The method for solving these equations is discussed by Coney and El-shaarawi [6].

3.2. Computing Temperature in the Flow Domain

The thermal part of the problem is solved using Equation (2.14) in the flow region. The finite difference form of the energy Equation (2.14) used by Hornbeck [12] is implemented.

$$U_{i,j}\frac{\theta_{i,j+1} - \theta_{i,j}}{\Delta X} + V_{i,j}\frac{\theta_{i+1,j+1} - \theta_{i-1,j+1}}{2\Delta R}$$
$$= \frac{1}{Pr}\left[\frac{\theta_{i+1,j+1} - 2\theta_{i,j+1} + \theta_{i-1,j+1}}{(\Delta R)^2} + \frac{1}{R_i}\frac{\theta_{i+1,j+1} - \theta_{i-1,j+1}}{2\Delta R}\right] \tag{3.5}$$

This equation is applied for $i = 1$ to n. At $R = 0$, apply the limiting process as $R \to 0$ i.e. for R=0

$$U_{0,j}\frac{\theta_{0,j+1} - \theta_{0,j}}{\Delta X} = \frac{4}{Pr}\frac{\theta_{1,j+1} - \theta_{0,j+1}}{(\Delta R)^2} \tag{3.6}$$

The Equations (3.5) and (3.6) simplify to:

$$\theta_{i-1,j+1}\left[-\frac{V_{i,j}}{2(\Delta R)} + \frac{1}{2Pr(\Delta R)R_i} - \frac{1}{Pr(\Delta R)^2}\right] + \theta_{i,j+1}\left[\frac{U_{i,j}}{\Delta X} + \frac{2}{Pr(\Delta R)^2}\right]$$

$$+ \theta_{i+1,j+1}\left[-\frac{1}{2Pr(\Delta R)R_i} + \frac{V_{i,j}}{2(\Delta R)} - \frac{1}{Pr(\Delta R)^2}\right] = \frac{U_{i,j}\theta_{i,j}}{\Delta X} \tag{3.7}$$

and

$$\theta_{0,j+1}\left[\frac{U_{0,j}}{\Delta X} + \frac{4}{Pr(\Delta R)^2}\right] + \theta_{1,j+1}\left[\frac{-4}{Pr(\Delta R)^2}\right] = \frac{U_{0,j}\theta_{0,j}}{\Delta X} \tag{3.8}$$

Under the constant wall temperature boundary condition, numerically solving the linear Equations (3.7) and (3.8) using the Gauss elimination method, the temperature at the j+1 level is determined. Continuing this process downstream allows us to analyze the thermal boundary layer within the flow domain.

For a constant wall heat flux condition. To solve this, the wall heat flux condition from Equation (2.18) provides the necessary additional equation, which is formulated using a finite difference approximation as follows:

$$\frac{3\theta_{n+1,j+1} - 4\theta_{n,j+1} + \theta_{n-1,j+1}}{2(\Delta R)} = 1 \tag{3.9}$$

where, $\theta_{n+1,j+1}$ represents the wall temperature. To analyze the thermal boundary layer under the constant wall heat flux condition, the temperature field is obtained by numerically solving Equations (3.7), (3.8), and (3.9).

3.3. Computing Heat Transfer Parameters

This section analyzes heat transfer parameters, including the local Nusselt Number at the wall and the bulk temperature, using the flow parameters within the flow domain.

The bulk temperature for this flow is given in [6],

$$T_b = \frac{\int_0^{r_1} 2\pi r v_x T \, dr}{\int_0^{r_1} 2\pi r v_x \, dr} \tag{3.10}$$

After non-dimensionality,

$$\theta_b = 2\int_o^R UR\theta \, dR \tag{3.11}$$

Here, θ_b is the non-dimensional bulk temperature. Applying Simpson's rule allows for the numerical calculation of the bulk temperature, which results in

$$\theta_b\Big|_{j+1} = \frac{2(\Delta R)}{3}\left(\sum_{i=1,3,5,7,9,\ldots}^{n} 4U_{i,j+1}R_i\theta_{i,j+1} + \sum_{i=2,4,6,8,\ldots}^{n-1} 2U_{i,j+1}R_i\theta_{i,j+1}\right) \tag{3.12}$$

The local Nusselt number is expressed as follows:

$$Nu_x = \frac{2hr_1}{k} \tag{3.13}$$

Two thermal boundary conditions were examined here: the Nusselt number for the corresponding boundary conditions:

For constant wall temperature,

$$h(T_w - T_b) = k\frac{\partial T}{\partial r} \tag{3.14}$$

$$Nu_x = \frac{-\frac{\partial T}{\partial r}\Big|_w 2r_1}{T_b - T_w} \tag{3.15}$$

and dimensionless form of Equation (3.15)

$$Nu_X\Big|_{j+1} = \frac{2\frac{\partial\theta}{\partial R}\Big|_w}{1-\theta_b} = \frac{2\left[\frac{3\theta_{n+1,j+1}-4\theta_{n,j+1}+\theta_{n-1,j+1}}{2(\Delta R)}\right]}{1-\theta_b|_{j+1}} \tag{3.16}$$

For constant wall heat flux,

$$h(T_w - T_b) = q \tag{3.17}$$

$$Nu_x = \frac{-q(2r_1)}{k(T_b - T_w)} \tag{3.18}$$

and dimensionless form of Equation (3.18),

$$Nu_X\Big|_{j+1} = \frac{-2}{(\theta_b - \theta_w)_{j+1}} \tag{3.19}$$

Equations (3.12), (3.16), and (3.19) are used to calculate heat transfer parameters of fluid flow in the domain. The graphical analysis of the flow parameters is detailed in the next section.

4. Results and Discussions

The governing equations were numerically resolved to evaluate the flow parameters, including velocities, pressure, and temperature, for various Bingham numbers (B=0,10,50) and Prandtl numbers (Pr=1,5,10).

4.1. Discussions on Velocity and Pressure in Flow domain.

In this section, velocity and pressure in the flow domain are analyzed. Figure 3 illustrates the development of axial velocity at different locations and for various values of Bingham numbers. This profile clearly shows the plug region of the Bingham fluid, and it becomes evident that as the Bingham number increases, the thickness of the plug also increases. This trend is consistently observed in the simulations for Bingham fluids modeled using the Papanastasiou regularization, with the exponent M set to 10,00,000. Figure 4 shows the fully developed velocity at the dimensionless axial location X = 0.25. It indicates that as the Bingham number rises, the maximum velocity decreases and the entry length—defined as the distance at which the velocity reaches 99% of its fully developed value—also decreases due to the formation of the plug region in the flow. On comparison, our results of velocity are found to be in agreement with the results obtained by Vradis et al. [33] for the fully developed case as depicted in Figure 5 and our results match the fully developed axial velocity profiles reported by Baioumy et al. [1].

Figure 6 illustrates the pressure drop along the axial direction, which decreases in the axial direction (X) of the cylinder from the entrance region. As the Bingham number increases, the pressure drop also decreases, which demonstrates that a higher yield stress fluid leads to a larger pressure drop. This is consistent with the previous results reported in [1].

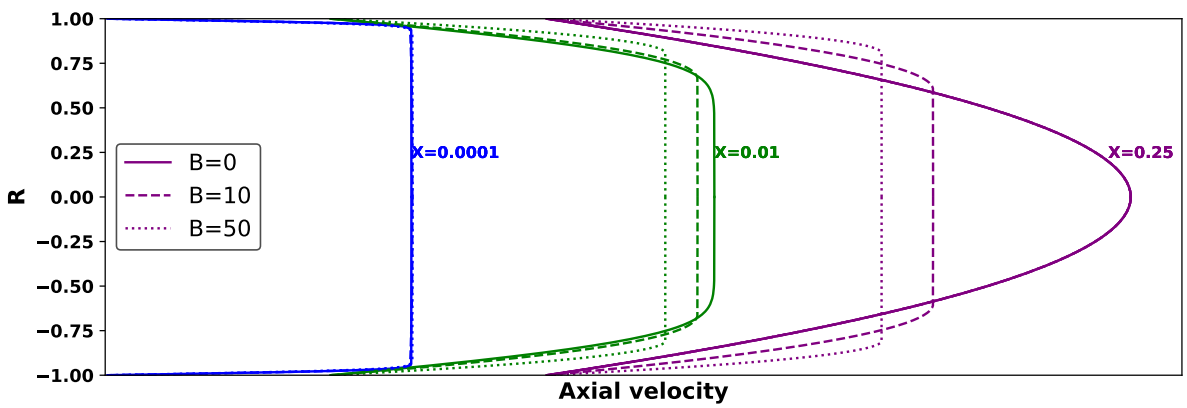

Figure 3: Fully developed axial velocity profile

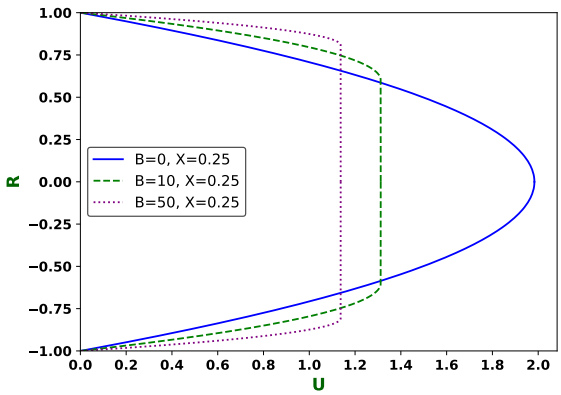

Figure 4: Axial velocity profile at X=0.25

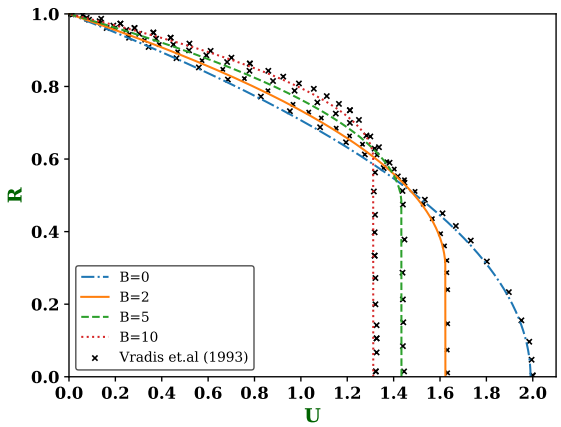

Figure 5: Comparing fully developed axial velocity profile with previous result of Vradis et al. [33]

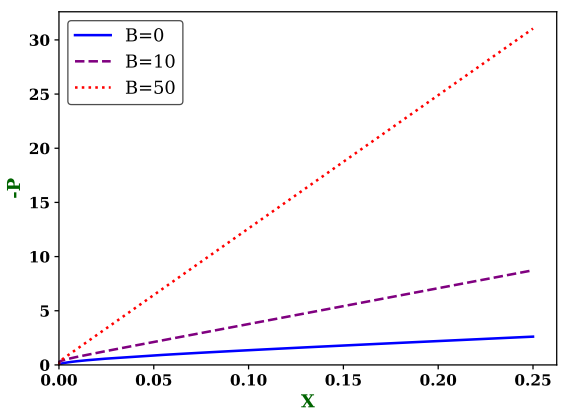

Figure 6: Pressure drop profile.

4.2. Discussions on Temperature profiles in Flow domain.

The results presented focus on the thermal boundary layer under two distinct boundary conditions: constant wall temperature and constant wall heat flux. Figure 7 shows the temperature profiles along the radial direction at a fixed axial location $X = 0.25$, for various Bingham numbers $B = (0, 10, 50)$ and Prandtl numbers $Pr = (1, 5, 10)$. Subfigures 7(a), 7(c), and 7(e) correspond to the constant wall temperature case, while Subfigures 7(b), 7(d), and 7(f) represent the constant wall heat flux condition. The temperature variation along the wall differs significantly between the two boundary conditions. In particular, for the constant wall heat flux case, higher Bingham numbers result in lower wall temperatures, as evident in Sub figures 7(b), 7(d), and 7(f). These results indicate that the thermal boundary layer extends farther downstream than the hydrodynamic boundary layer, especially at higher Prandtl numbers.

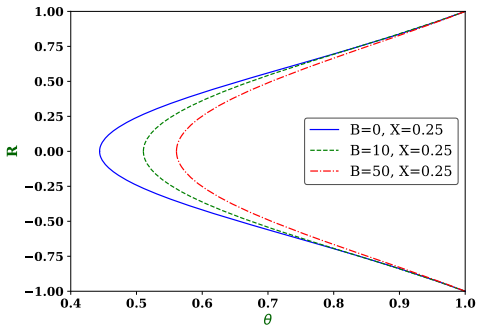

(a) Pr = 1

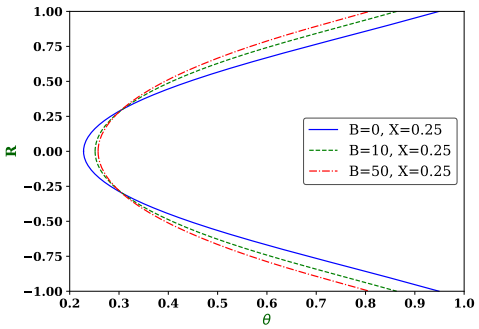

(b) Pr = 1

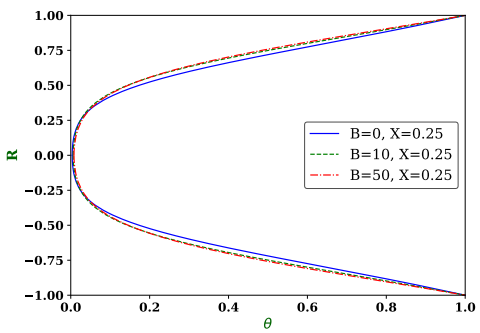

(c) Pr = 5

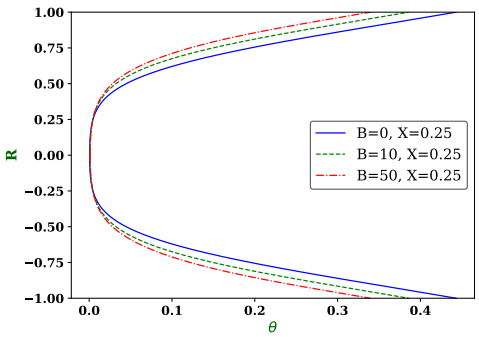

(d) Pr = 5

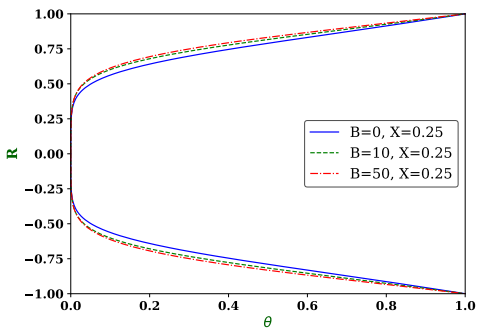

(e) Pr = 10

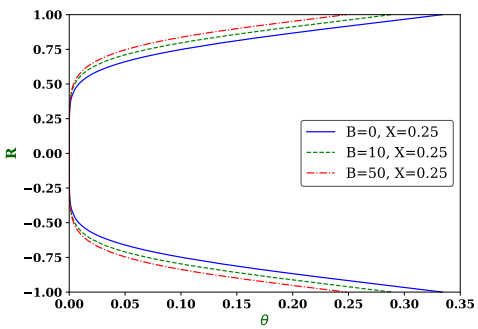

(f) Pr = 10

Figure 7: Comparison of temperature for different Prandtl numbers (Pr = 1, 5, 10) under two thermal boundary conditions: (7a,7c,7e) constant wall temperature, and (7b,7d,7f) constant wall heat flux.

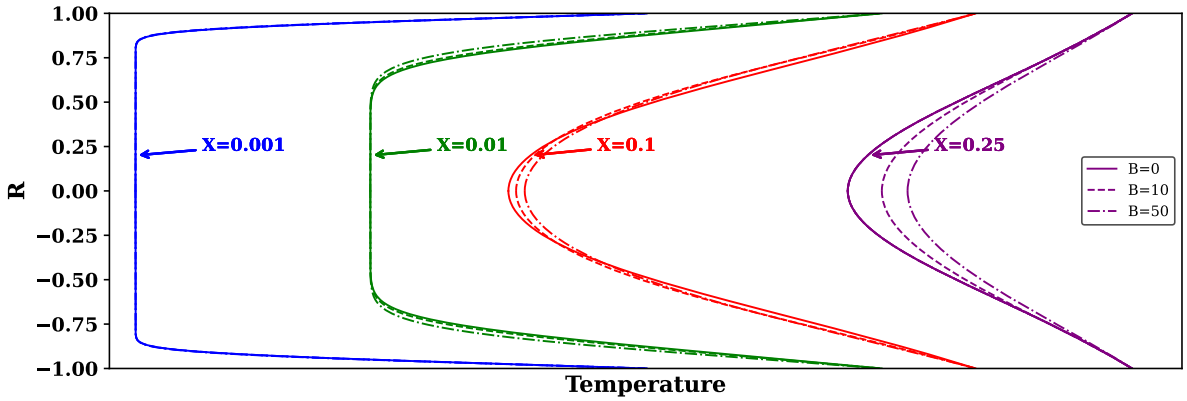

Figure 8: Temperature profile with constant wall temperature and Pr=1

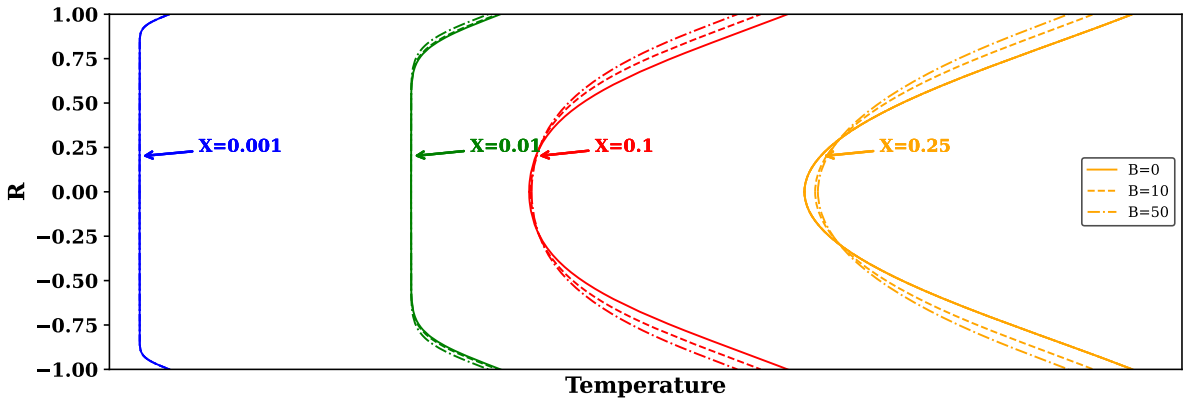

Figure 9: Temperature profile with constant wall heat flux and Pr=1

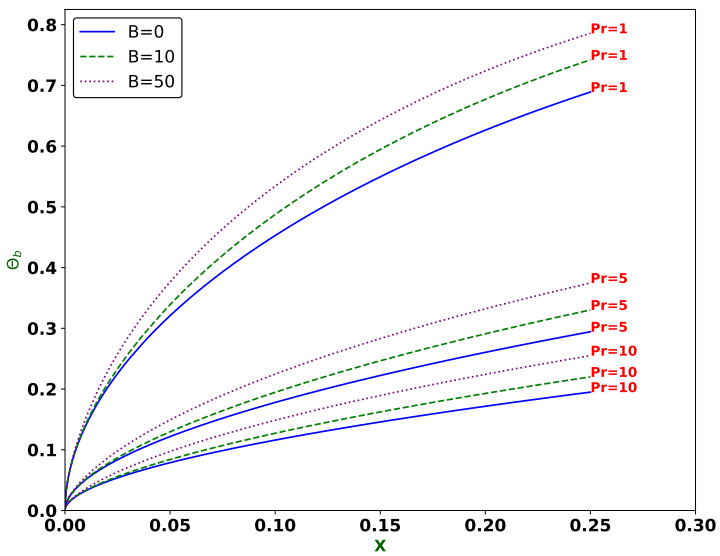

Figure 10: Bulk temperature for different Prandtl numbers (Pr = 1, 5, 10) under constant wall temperature condition

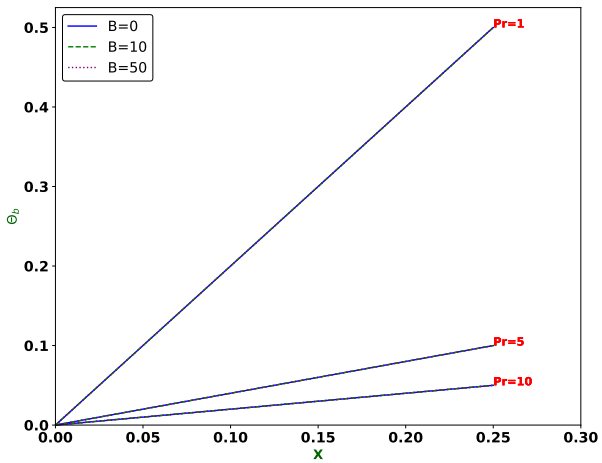

Figure 11: Bulk temperature for different Prandtl numbers (Pr = 1, 5, 10) under constant wall heat flux condition

The development of temperature profiles along radial direction at some axial locations for various Bingham numbers $B = (0, 10, 50)$ and Prandtl number $Pr = 1$ are illustrated in Figure 8 for the constant wall temperature case, and in Figure 9 for the constant heat flux case.

4.3. Heat Transfer Parameters

The commonly analyzed heat transfer parameters in the study of boundary layers are bulk temperature, wall temperature, and Nusselt number, which will be discussed in the following two sections.

4.3.1. ***Bulk Temperature and Wall Temperature.*** For the constant wall temperature condition, the bulk temperature θ_b varies nonlinearly along the axial direction X for different Bingham numbers and Prandtl numbers. The influence of both the Bingham number and the Prandtl number is more pronounced in this case. Specifically, the bulk temperature increases with increasing Bingham number, and for a fixed Bingham number, lower Prandtl numbers result in higher bulk temperatures due to greater thermal diffusivity. These trends are illustrated in Figure 10.

In contrast, under the constant wall heat flux condition, the bulk temperature increases nearly linearly along the axial direction as seen in Figure 11. The effect of the Bingham number on bulk temperature is minimal, but the Prandtl number still plays a role—higher Prandtl numbers lead to lower bulk temperatures, attributed to lower thermal diffusivity and a thinner thermal boundary layer. Additionally, for this case, the wall temperature varies axially, and the lower Bingham number results in a higher wall temperature compared to a larger Bingham number, as shown in Figure 12 for different Prandtl numbers.

Figure 13 illustrates the variation of the dimensional bulk temperature with the dimensional axial distance(X) for different Bingham numbers, corresponding to three Prandtl numbers (1, 5, 10), under the constant wall temperature. It is evident from Figure 13 that the bulk temperature is lower for smaller Bingham numbers compared to higher ones. Moreover, the difference between these cases becomes more pronounced as the Prandtl number increases.

4.3.2. ***Nusselt Number.*** Figure 14 illustrates how the local Nusselt number varies along the axial direction of the cylinder under these two distinct boundary conditions: constant wall temperature, as shown in Subfigures 14(a), 14(c), 14(e), and constant wall heat flux, as seen in Subfigures 14(b), 14(d), 14(f). The analysis takes into account three different Prandtl numbers (1, 5, and 10) and three different Bingham numbers (0, 10, and 50).

In each scenario, a higher Bingham number correlates with a greater local Nusselt number compared to a lower Bingham number due to decreases in axial conduction for larger yield stress. This observation indicates that the local heat transfer rate per unit area is higher for more viscous fluids, as indicated by the Bingham number. Additionally, at the cylinder entrance, the local Nusselt number is higher when a

greater Prandtl number is present. This behavior is associated with the formation of the thermal boundary layer, demonstrating that heat transfer is more significant at the entrance and gradually decreases as the flow develops. The percentage increase in between the yield stress fluid and Newtonian fluid Nusselt number increases with the Bingham number as shown in Figure 15.

Furthermore, when comparing the results under both thermal boundary conditions, the Nusselt number is observed to be higher under the constant wall heat flux condition. This discrepancy arises from the boundary condition at the wall, which influences the Nusselt number. The corresponding values of the Nusselt number for different Bingham and Prandtl numbers are summarized in Table 1.

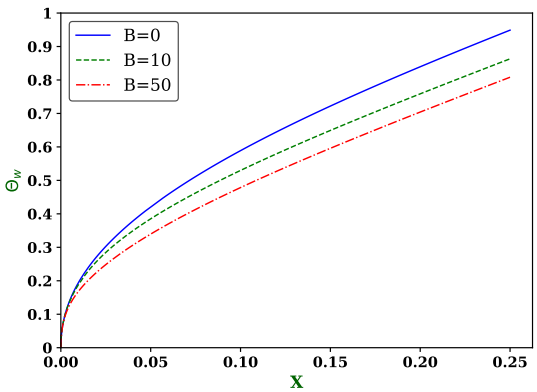

(a) Pr = 1

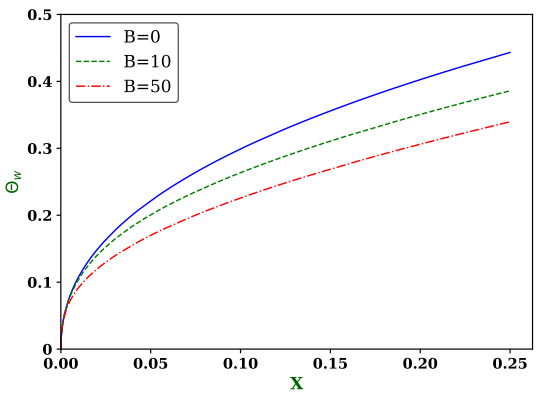

(b) Pr = 5

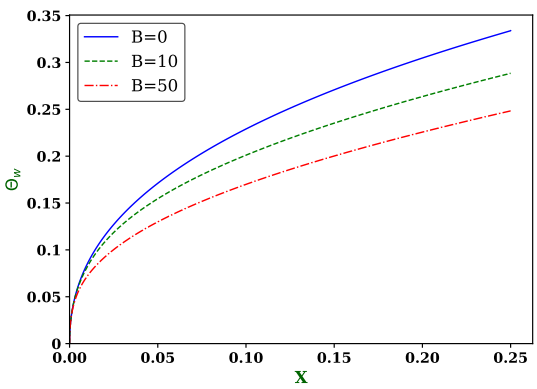

(c) Pr = 10

Figure 12: Wall temperature of a constant wall heat flux boundary condition.

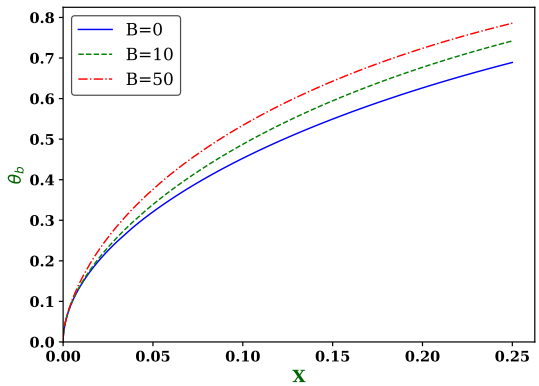

(a) Pr=1

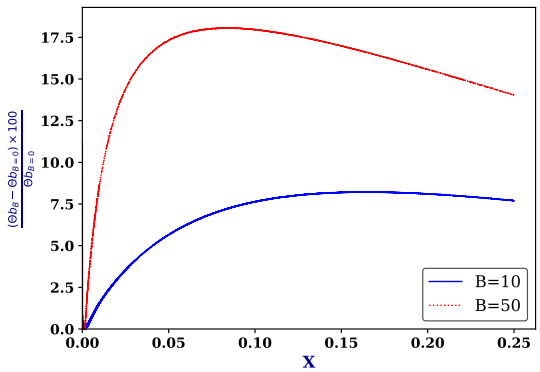

(b) Pr=1

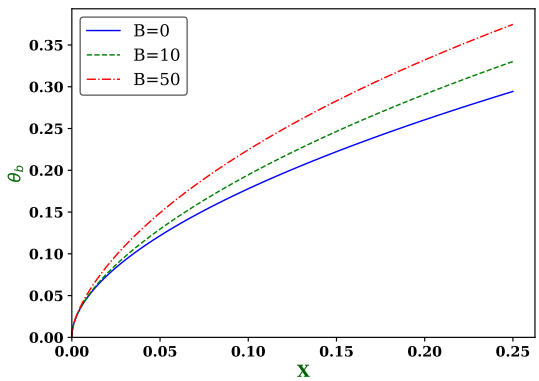

(c) Pr=5

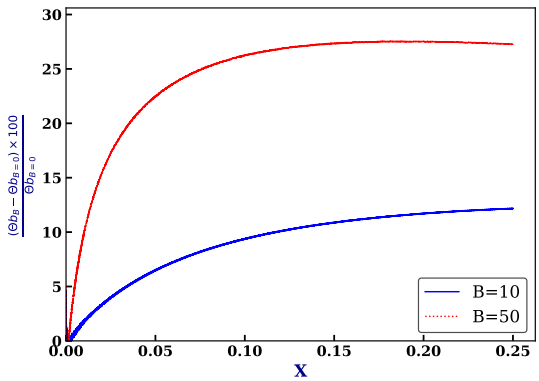

(d) Pr=5

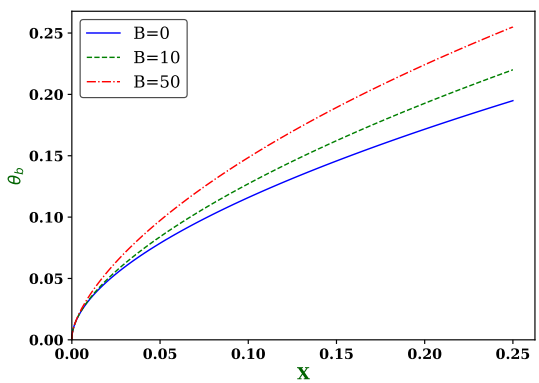

(e) Pr=10

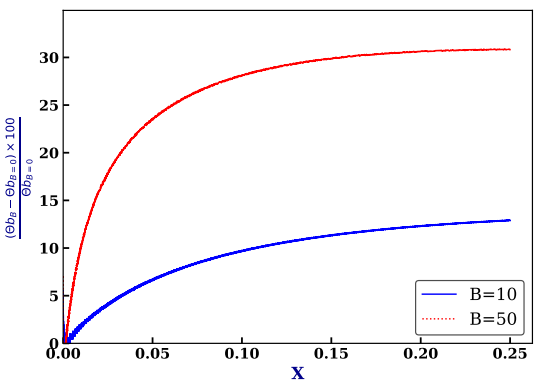

(f) Pr=10

Figure 13: Bulk temperature for different Prandtl numbers 1,5,10 and constant wall temperature condition shows in Figures (13a,13c,and13e) and percentage increase in bulk temperature with respect to Newtonian fluids shows in Figures (13b, 13d, and 13f).

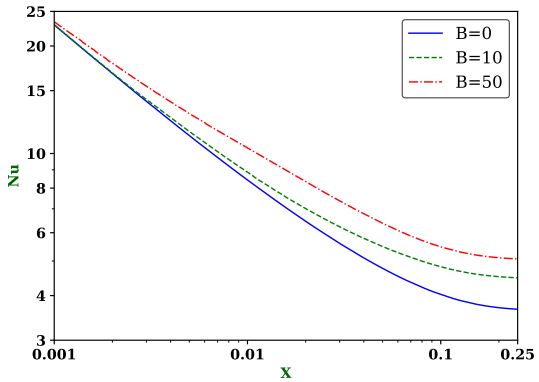

(a) Pr = 1

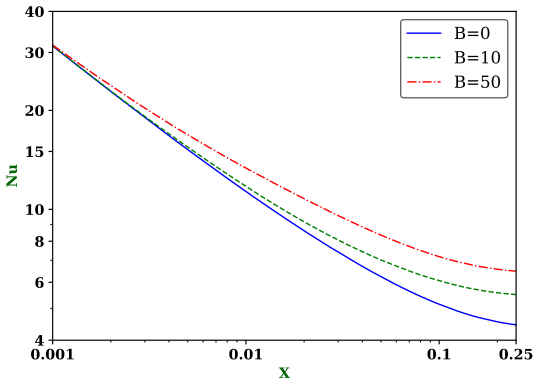

(b) Pr = 1

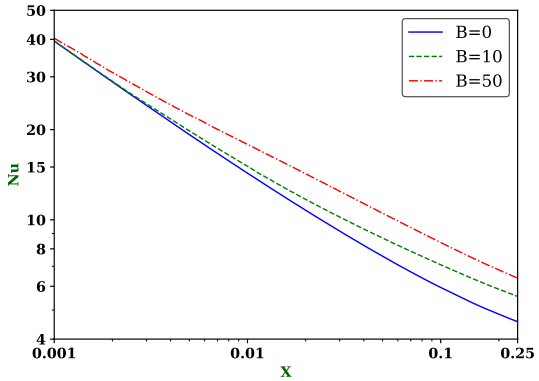

(c) Pr = 5

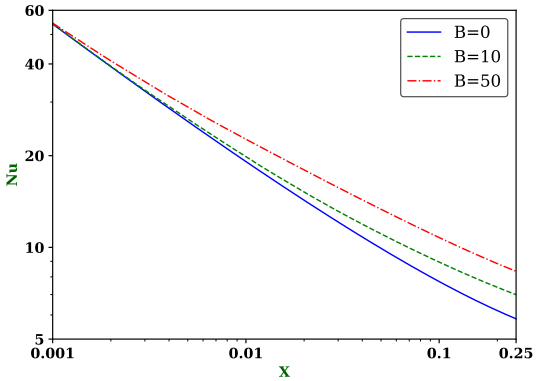

(d) Pr = 5

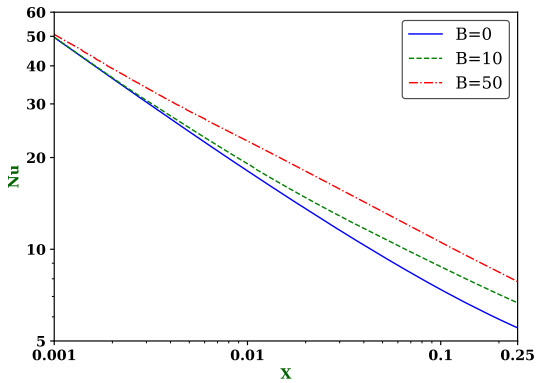

(e) Pr = 10

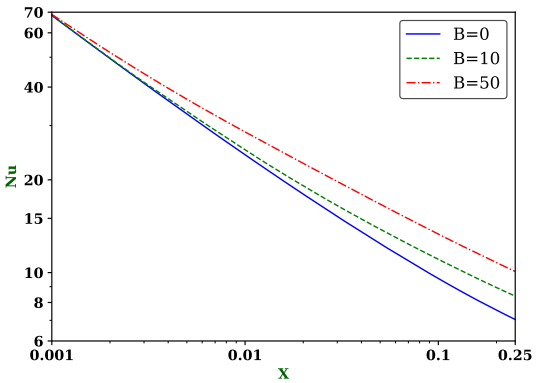

(f) Pr = 10

Figure 14: Comparison of Nusselt number for different Prandtl numbers (Pr = 1, 5, 10) under two thermal boundary conditions: (14a, 14c, 14e) constant wall temperature, and (14b, 14d, 14f) constant heat flux. The results highlight the effect of boundary conditions and fluid properties on convective heat transfer.

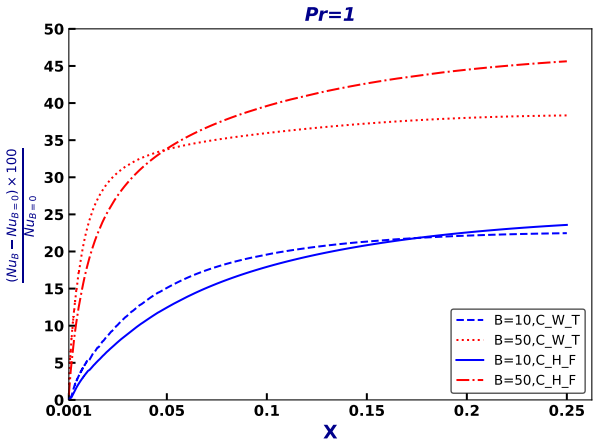

(a) Pr = 1

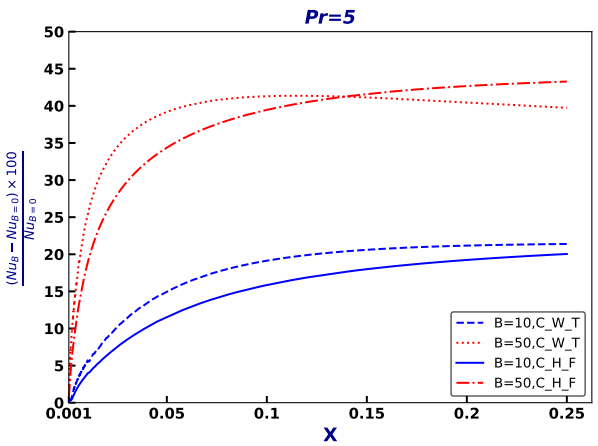

(b) Pr = 5

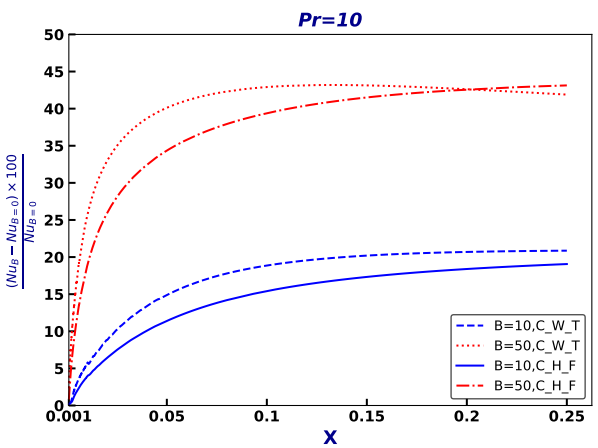

(c) Pr = 10

Figure 15: Percentage increase in Nusselt number with respect to Newtonian fluid (B=0) for different Bingham numbers (B=10,50) and different Prandtl numbers (Pr = 1, 5, 10) under two thermal boundary conditions.

Table 1: Nusselt number for different Prandtl and Bingham numbers under two thermal boundary conditions

Pr	x	Constant Wall Temperature			Constant Wall Heat Flux		
		$B = 0$	$B = 10$	$B = 50$	$B = 0$	$B = 10$	$B = 50$
1	0.001	22.9161	22.9513	23.3818	31.3986	31.4441	31.5995
	0.01	8.4301	8.8685	10.3672	11.3348	11.7554	13.3557
	0.25	3.6622	4.4851	5.0662	4.4554	5.5061	6.4883
5	0.001	39.4624	39.5348	40.3562	54.0602	54.1557	54.4742
	0.01	14.3098	15.0910	17.8731	19.1248	19.8524	22.6481
	0.25	4.5742	5.5524	6.3919	5.8276	6.9954	8.3494
10	0.001	49.5886	49.6859	50.7451	68.3139	68.4412	68.8622
	0.01	18.0801	19.0842	22.6615	24.1224	25.0516	28.6141
	0.25	5.5193	6.6708	7.8315	7.0456	8.3884	10.0844
100	0.001	99.8195	100.0658	102.0181	147.6267	147.9271	148.7712
	0.01	38.8837	41.1450	49.1666	52.4835	54.5711	62.5208
	0.25	11.6433	13.9536	16.8664	14.7315	17.3407	20.9828

5. Conclusion

The computational investigation focuses on the simultaneous development of hydrodynamic and thermal boundary layers at a cylindrical entrance for the incompressible, laminar flow of a viscoplastic Bingham fluid, utilizing the regularized Bingham-Papanastasiou model. In this study, a finite difference method is employed to solve the governing Prandtl boundary layer equations.

We analyzed the hydrodynamic solution in terms of velocity profiles and pressure drop distributions in the entrance region of the cylinder, and the results are concluded as follows:

- Similar to Newtonian fluids, Bingham fluids display velocity overshoots in the entrance region of the cylinder; however, the magnitude of these overshoots decreases as the Bingham number increases..
- The Bingham number significantly influences the pressure drop along the axial direction in the flow domain.

The thermal boundary layer parameters were analyzed under two distinct thermal boundary conditions: constant wall temperature and constant wall heat flux. This study investigates heat transfer characteristics, including bulk temperature, wall temperature, and the local Nusselt number, all of which are affected by variations in the Bingham number and Prandtl number. The key findings are summarized as follows:

- The bulk temperature is higher for a greater Bingham number compared to a lower one under the thermal boundary condition of constant wall temperature; bulk temperature changes are negligible in the case of constant wall heat flux with respect to Bingham number.
- In examining both thermal boundary conditions, we find that in the entrance region, the Nusselt number remains nearly the same for all Bingham numbers, indicating that it is not dependent on the Bingham number in this region. However, beyond a certain axial location, the Nusselt number for Bingham fluids surpasses that of Newtonian fluids, enhancing the local heat transfer rate at those points.
- A comparison of the local Nusselt number for both thermal boundary conditions reveals that it is consistently higher under the constant wall heat flux condition compared to the constant wall temperature condition.

Acknowledgments

We thank the organizers of the "International Conference on Mathematical Sciences and Computing Innovations and Applications (ICMSC-2025) jointly organized by Department of Mathematics North Eastern Regional Institute of Science and Technology (NERIST) and Department of Mathematics National institute of technology (NIT), Uttarakhand,India held over June 26-28, 2025.

References

1. Basma Baioumy, Rachid Chebbi, and Nabil Abdel Jabbar. Bingham fluid flow in the entrance region of a pipe. *Journal of Fluids Engineering*, 143(2):024503, 2021.

2. Ali Belhocine, Mohammed Sid Ahmed Houari, Nadica Stojanovic, and Oday Ibraheem Abdullah. Numerical analysis of heat transfer in simultaneously developing laminar flow in a plane duct with constant wall temperature and heat flux boundary conditions. *Heat Transfer*, 2025.

3. Abdelhamid Boualit, Noureddine Zeraibi, Sabrina Boualit, and Meriam Amoura. Thermal development of the laminar flow of a bingham fluid between two plane plates with viscous dissipation. *International Journal of Thermal Sciences*, 50(1):36–43, 2011.

4. Rachid Chebbi. Viscous dissipation effects and developing heat transfer for fully developed power-law fluid flow in the entrance region of a tube. *Energies*, 18(6):1357, 2025.

5. Rachid Chebbi, Habib H Al-Ali, and M Sami Selim. Simultaneously developing laminar flow and heat transfer in the entrance region of a circular tube with constant wall temperature. *Chemical Engineering Communications*, 160(1):59–70, 1997.

6. JER Coney and MAI El-Shaarawi. Finite difference analysis for laminar flow heat transfer in concentric annuli with simultaneously developing hydrodynamic and thermal boundary layers. *International Journal for numerical methods in engineering*, 9(1):17–38, 1975.

7. F Durst, Subhashis Ray, Bülent Ünsal, and OA Bayoumi. The development lengths of laminar pipe and channel flows. *Journal of fluid Engineering*, 127(6):1154–1160, 2005.

8. Marilize Everts, Mostafa Mahdavi, Josua P Meyer, and Mohsen Sharifpur. Development of the hydrodynamic and thermal boundary layers of forced convective laminar flow through a horizontal tube with a constant heat flux. *International Journal of Thermal Sciences*, 186:108098, 2023.

9. Marilize Everts and Josua P Meyer. Laminar hydrodynamic and thermal entrance lengths for simultaneously hydrodynamically and thermally developing forced and mixed convective flows in horizontal tubes. *Experimental Thermal and Fluid Science*, 118:110153, 2020.

10. Evgenios Gryparis, Alexandros Syrakos, and Georgios C Georgiou. Bingham flow development in annular tubes in the presence of wall slip. *Journal of Non-Newtonian Fluid Mechanics*, 339:105418, 2025.

11. Muhammad Faheem Hassan and Rachid Chebbi. Analysis of heat transfer for simultaneously developing temperature profile and fluid flow of power-law fluids in the entrance region of a tube. *International Journal of Thermofluids*, 16:100240, 2022.

12. Robert W Hornbeck. Laminar flow in the entrance region of a pipe. *Applied Scientific Research, Section A*, 13:224–232, 1964.

13. Yash Joshi and BR Vinoth. Entry lengths of laminar pipe and channel flows. *Journal of Fluids Engineering*, 140(6):061203, 2018.

14. Sadik Kakac, Yaman Yener, and Anchasa Pramuanjaroenkij. *Convective Heat Transfer*. CRC Press, Boca Raton, 2013.

15. A Kandasamy and Srinivasa Rao Nadiminti. Entrance region flow in concentric annuli with rotating inner wall for herschel–bulkley fluids. *International Journal of Applied and Computational Mathematics*, 1(2):235–249, 2015.

16. Nabila Labsi, Youb Khaled Benkahla, and Abdelkader Boutra. Viscous dissipation effect on the flow of a thermodependent herschel-bulkley fluid. *Thermal Science*, 19(5):1553–1564, 2015.

17. Nabila Labsi, Youb Khaled Benkahla, Abdelkader Boutra, and Abdellah Ammouri. Heat and flow properties of a temperature dependent viscoplastic fluid including viscous dissipation. *Journal of Food Process Engineering*, 36(4):450–461, 2013.

18. Taegee Min, Hyoung Gwon Choi, Jung Yul Yoo, and Haecheon Choi. Laminar convective heat transfer of a bingham plastic in a circular pipe—ii. numerical approach hydrodynamically developing flow and simultaneously developing flow. *International Journal of Heat and Mass Transfer*, 40(15):3689–3701, 1997.

19. Evan Mitsoulis and RR Huilgol. Entry flows of bingham plastics in expansions. *Journal of non-newtonian fluid mechanics*, 122(1-3):45–54, 2004.

20. Srinivasa Rao Nadiminti and A Kandasamy. Entrance region flow in concentric annuli with rotating inner wall for bingham fluid. *Journal of Computational and Applied Mechanics*, 11(2):137–157, 2016.

21. N Nirmalkar, RP Chhabra, and RJ Poole. Laminar forced convection heat transfer from a heated square cylinder in a bingham plastic fluid. *International Journal of Heat and Mass Transfer*, 56(1-2):625–639, 2013.

22. Z Nowak and B Gajdeczko. Laminar entrace region flow of the bingham fluid. *Acta mechanica*, 49(3):191–200, 1983.

23. Shinichi Ookawara, Kohei Ogawa, Norman Dombrowski, Esmail Amooie-Foumeny, and Ahmed Riza. Unified entry length correlation for newtonian, power law and bingham fluids in laminar pipe flow at low reynolds number. *Journal of Chemical Engineering of Japan*, 33(4):675–678, 2000.

24. Rekha G Pai and A Kandasamy. Entrance region flow of herschel-bulkley fluid in an annular cylinder. *Applied Mathematics*, 5(13):1964–1976, 2014.

25. TC Papanastasiou and AG Boudouvis. Flows of viscoplastic materials: models and computations. *Computers & Structures*, 64(1-4):677–694, 1997.

26. Maria Philippou, Zacharias Kountouriotis, and Georgios C Georgiou. Viscoplastic flow development in tubes and channels with wall slip. *Journal of non-newtonian fluid mechanics*, 234:69–81, 2016.

27. RJ Poole and RP Chhabra. Development length requirements for fully developed laminar pipe flow of yield stress fluids. *Journal of fluid Engineering*, 132(3):034501, 2010.

28. Åsmund Aamodt Resell, Knut Erik Teigen Giljarhus, and Hans Joakim Skadsem. Entrance lengths for fully developed laminar flow in eccentric annulus. *Journal of Fluids Engineering*, 147(5), 2025.

29. Edson J Soares, Mônica F Naccache, and Paulo R Souza Mendes. Heat transfer to viscoplastic materials flowing axially through concentric annuli. *International Journal of Heat and Fluid Flow*, 24(5):762–773, 2003.

30. Márcia Soares, Mônica F Naccache, and Paulo R Souza Mendes. Heat transfer to viscoplastic materials flowing laminarly in the entrance region of tubes. *International journal of heat and fluid flow*, 20(1):60–67, 1999.

31. V. R. Sudarsan. *On Development of Numerical Techniques and Algorithms for Non-Newtonian Fluid Flow Problems and Rheodynamic Lubrication of Porous Rollers*. PhD thesis, 1991. AAI30273756.

32. Alexandros Syrakos, Evgenios Gryparis, and Georgios C Georgiou. A revisit of the development of viscoplastic flow in pipes and channels. *Journal of Non-Newtonian Fluid Mechanics*, 334:105341, 2024.

33. George C Vradis, John Dougher, and Sunil Kumar. Entrance pipe flow and heat transfer for a bingham plastic. *International journal of heat and mass transfer*, 36(3):543–552, 1993.

34. MAO Zaisha, YANG Chao, and C Kelessidis Vassilios. Modeling and numerical simulation of yield viscoplastic fluid flow in concentric and eccentric annuli. *Chinese Journal of Chemical Engineering*, 20(1):191–202, 2012.

Deepa Madivalar,
Department of Mathematical and Computational Sciences,
National Institute of Technology Karnataka Suratkal,Mangalore,575025,
India.
E-mail address: d.227ma009@nitk.edu.in

and

Vishwanath Kadaba Puttanna,
Department of Mathematical and Computational Sciences,
National Institute of Technology Karnataka Suratkal,Mangalore,575025,
India.
E-mail address: vishy@nitk.edu.in

and

A. Kandasamy,
Department of Mathematical and Computational Sciences,
National Institute of Technology Karnataka Suratkal,Mangalore,575025,
India.
E-mail address: kandy@nitk.edu.in